Tectonic activity along the inner margin of the South Tibetan Detachment constrained by syntectonic leucogranite emplacement in Western Bhutan

Accepted Manuscript

Tectonic activity along the inner margin of the South Tibetan detachment constrained by syntectonic leucogranite emplacement in Western Bhutan

Chiara Montomoli, Rodolfo Carosi, Daniela Rubatto, Dario Visonà, Salvatore Iaccarino

To appear in: *Italian Journal of Geosciences*

Received date: 29 June 2015

Accepted date: 26 September 2015

doi: 10.3301/IJG.2015.26

Please cite this article as:

C. Montomoli, R. Carosi, D. Rubatto, D. Visonà, S. Iaccarino - Tectonic activity along the inner margin of the South Tibetan detachment constrained by syntectonic leucogranite emplacement in Western Bhutan, Italy, *Italian Journal of Geosciences* 10.3301/IJG.2015.26

TECTONIC ACTIVITY ALONG THE INNER MARGIN OF THE SOUTH TIBETAN DETACHMENT CONSTRAINED BY SYNTECTONIC LEUCOGRANITE EMPLACEMENT IN WESTERN BHUTAN

C. MONTOMOLI [1], R. CAROSI [2], D. RUBATTO [3], D. VISONÀ [4], S. IACCARINO [1]

[1] Dipartimento di Scienze della Terra, via S. Maria, 53, 56126, Pisa, Italy
[2] Dipartimento di Scienze della Terra, via Valperga Caluso, 35, 10125, Torino, Italy
[3] Research School of Earth Sciences, Australian National University, Canberra, Australia
[4] Dipartimento di Geoscienze, via Gradenigo 6, 35131, Padova, Italy.

Abstract

In Western Bhutan Himalayas leucogranite dykes emplaced in sub-vertical hybrid fractures that cut across the high-grade rocks of the upper Greater Himalayan Sequence just below to the South Tibetan Detachment. The granitic dykes dip to the North often showing a mylonitic deformation with a top-down to-the-N sense of shear. The high-angle fractures are interpreted to be related to the evolution of the South Tibetan Detachment toward a brittle regime of deformation. U-Pb monazite ages constrain the leucogranite emplacement at 13.9±06 Ma implying that brittle-ductile deformation of the South Tibetan Detachment was active at that time. NNE-SSW to nearly E-W trending large scale antiforms and synforms mapped in NW Bhutan affected the Greater Himalayan Sequence and South Tibetan Detachment only after 14 Ma.

Key-words: South Tibetan Detachment System, leucogranite, Bhutan himalaya

Introduction

The Greater Himalayan Sequence (GHS) is the metamorphic core of the Himalayan belt (Fig. 1) and consists of medium to high-grade metamorphic rocks widely intruded by Miocene leucogranites in its upper portion (the upper GHS, GHSu) (DEBON *et alii*, 1986; VISONÀ & LOMBARDO; 2002; VISONÀ *et alii*, 2012; SEARLE, 2013). Leucogranites form both large-size granitic plutons such as the Makalu (STREULE *et alii*, 2010), Manaslu (GUILLOT *et alii*, 1994),

Nuptse (Jessup *et alii*, 2008) and Bura Buri (Carosi *et alii*, 2013) and smaller sized melts whose emplacement was controlled by tectonic structures (Searle *et alii*, 2010). The volume of syn-orogenic granites varies along the strike of the belt, reaching greatest volumes in the eastern part of the Himalayas (Leech, 2008 with references).

Himalayan leucogranites are commonly subdivided in two groups: (i) biotite or two mica granite (± tourmaline ± cordierite ± sillimanite ± andalusite ± kyanite ± garnet) and (ii) tourmaline granite (± andalusite ± sillimanite ± garnet). In Bhutan, leucogranites intruded in the upper GHS and in the overlying Checkha Formation between 24-17 Ma (Edwards & Harrison, 1997; Visonà & Lombardo 2002; Visonà *et alii*, 2012; Grujic *et alii,* 2002; Kellett *et alii*, 2010). The origin of these leucogranites is attributed to decompression melting at 25-11 Ma during the exhumation of the GHS (Harris & Massey, 1994; Patiño-Douce & Harris, 1998; Searle, 2013). In addition to this, recent reports of melt inclusions of tonalitic compositions within garnets of the GHS in Central Nepal that formed at ~41-36 Ma (Carosi *et alii*, 2015; Iaccarino *et alii,* 2015) suggest that melts were also present at peak metamorphic conditions (King *et alii*, 2011).

Geological investigations in Western Bhutan have recognized two different generations of Higher Himalayan leucogranites emplaced in the GHS, characterized by different age and tectonic setting. (1) A first generation of concordant leucogranites intruded the core of the GHS (Gasa-Koina-Laya area; Fig. 2) at 20-17 Ma (Carosi *et alii*, 2006). Their emplacement and cooling are closely related to the development of high-grade, ductile and normal-sense shear zones with a top-to–the SE sense of shear (Carosi *et alii*, 2006). The normal-sense shear zones have been interpreted to accommodate the lengthening of the inner part of the GHS in response to the pure shear component of the flow as indicated by kinematic vorticity analysis (Carosi *et alii*, 2006; Law *et alii*, 2004; Larson & Godin, 2009). (2) A second generation of leucogranite dykes have been found northeast of Laya village in Western Bhutan (Fig. 1; Fig. 2) associated with a system of high-angle fractures, with a width of few meters and length of several hundred meters, that occur just below the South Tibetan Detachment (STD) and above the Laya Thust (Grujic *et alii*, 2011). Regarding the second group, because of their defined structural position, geochronology of leucogranites has been used to constrain the age of STD in the inner part of the belt (inner STD; Kellett *et alii*, 2009, 2010).

The GHS as well as its tectonic boundaries (i.e. the Main Central Thrust and STD) were later deformed in a system of large-scale antiforms and synforms occurring at the regional scale (Carosi *et alii*, 1999). This late folding event is responsible for the formation of outer klippen of GHS and overlying Tibetan Sedimentary Sequence cropping out in the frontal part

of the belt. Once these late antiforms and synforms were activated, slip movements along the STDS became difficult and deformation retreated to the inner part of the belt (KELLET *et alii*, 2009). Despite the regional importance of this "late" folding event in shaping the frontal part of the belt, its timing is still poorly investigated. In this framework, we describe the structural position and constrain the chemistry and emplacement age of the leucogranite dykes in the nearly vertical fractures and in turn provide a lower limit for the timing of the large scale folding event.

Geological background

The Himalayan belt is characterized by the occurrence of a system of top-to-the North normal-sense ductile to brittle shear zones putting into contact the upper low-grade Paleozoic-Mesozoic rocks of the Tethyan Sedimentary Sequence (TSS) with the tectonically lower medium- to high-grade metamorphic rocks of the Greater Himalayan Sequence (GHS) (BURCHFIEL *et alii*, 1992; BURG *et alii*, 1984; CABY *et alii*, 1983; CAROSI *et alii*, 1998; SEARLE, 1999; SEARLE *et alii*, 2003). This system, known as the South Tibetan Detachment System (STDS), extends for almost the entire 2400 km length of the Himalayan belt.

Two major discontinuities are recognized as having a major role in the tectonic mechanisms invoked for the exhumation of the GHS; they are the STDS and the lower Main Central Thrust (MCT), a ductile shear zone separating the GHS from the structurally lower Lesser Himalayan Sequence (LHS). Tectonic models of channel flow (BEAUMONT *et alii*, 2001), critical taper (KOHN, 2008), wedge insertion (WEBB *et alii*, 2007) and wedge extrusion (HODGES *et alii*, 1992, GRUJIC *et alii*, 1996, VANNAY & GRASEMAN, 2001; GOSCOMBE *et alii*, 2006) all refer to these two major discontinuities. More recently it has been proposed that tectonic and metamorphic discontinuities within the GHS, and older than the MCT, divide this high-grade unit in two portions: a lower and an upper GHS (GHSl and GHSu; MONTOMOLI *et alii*, 2013, 2015). The existence of such intermediate discontinuities puts into questions models based only on MCT and STDS (*e.g.* MONTOMOLI *et alii*, 2015).

In central Nepal, the STDS was initially defined as a brittle fault (BURCHFIEL *et alii*, 1992) and later recognized as a system made by a lower ductile shear zone and an upper brittle fault (CAROSI *et alii*, 1998). However, along the belt and depending on the structural level of the exposed STDS, the ductile shear zone is always recognizable whereas the upper brittle fault is

sometimes lacking or not exposed (COTTLE *et alii*, 2007; KELLETT & GRUJIC, 2012).

In nearby Bhutan, KELLETT *et alii* (2009, 2010) recognised a different architecture of the STDS in a N-S section from the orogenic front to the inner portion of the belt where the portion of the discontinuity closer to orogenic front is called outer STDS whereas the internal portion is called inner STDS. They define the outer STDS as mainly a ductile shear zone that is not affected by brittle faults and is folded in synformal klippen. The outer STDS is traceable all along the belt and it better preserves the Miocene ductile structures of the STDS. According to KELLETT *et alii* (2010), ductile shearing is temporally constrained between c. 23 to 16 Ma, following the peak metamorphism in the GHS and Chekha formation. The inner STDS is a younger ductile to brittle shear zone active in more recent times with respect to the outer STDS (KELLETT *et alii*, 2009; 2010). According to KELLETT *et alii* (2009) the normal sense of shear of the inner STDS could be related to out-of-sequence thrusting along the Kakhtang thrust (DANIEL *et alii*, 2003) allowing the extrusion of the hanging wall of that thrust.

Along the strike of the belt, the geometry and age of the STDS appear to be more complicated. In Western Nepal a large body of High Himalayan leucogranite has been found intruding the STD at ~24-25 Ma in the inner portion of the belt with no evidences of later brittle reactivation (CAROSI *et alii*, 2013). On the other hand, younger ages at ~ 16 Ma for the ductile strand of the STD have been recently reported by COTTLE *et alii* (2015) in the Mt. Everest section pointing out the lack of a continuous and contemporaneous STD structure along the strike of the Himalaya (KELLETT *et alii*, 2013).

Structural setting

The study area is located in the upper portion of the GHS just below the lower ductile portion the STDS, i.e. near the boundary between Chekha formation and garnet and sillimanite-bearing gneisses of the GHS (Fig. 2). In the area between Sinche La (pass) and Laya village (Fig. 2) a system of a dozen of high-angle leucogranite dykes has been recognised (Fig. 3a and b).

The dykes are emplaced in a system of fractures striking E-W and steeply dipping to the N and NE (~ 80°) with a steeply plunging to moderately oblique mineral lineation. The fractures are hybrid fractures showing both sub-horizontal extension and shearing (RAMSEY & CHESTER, 2004). Sense of shear is highlighted by the drag of the foliation in the host gneiss at the mesoscale. At microscale leucogranites often show-solid state deformation and mylonitic texture with microscale kinematic indicators such as mica fish (Fig. 4a) and sigma - type

rotated porhyroclasts. Both meso- and microscale observations indicate that sense of shear is top-down-to-the N and NE (Fig. 4a and b). The stretching lineation is nearly down-dip indicating a minor component of horizontal displacement.

Petrology and Geochemistry

The leucogranite dikes include two-mica leucogranite, pegmatite and locally two-mica granite with layers or pegmatitic pockets. The two-mica granites are fine-grained and exhibit an equal amount of biotite and muscovite. The foliated leucogranites show intergranular fibrolite developed after muscovite.

Sample 10-41 (coordinates N28°03'47.7'' E089°35'27.3'', altitude 4300 m.a.s.l.) is a mylonitic leucogranite filling a high-angle fractures in biotite - sillimanite bearing gneiss of the GHS in Limithang area (Figs. 2, 3).

In this paper we compare sample 10-41 with previously published geochemical analyses of a two-mica mylonitic leucogranite (sample 10-53) and a weakly deformed biotite tourmaline-bearing leucogranite (sample 10-56) dated at ~ 17 and ~ 20, Ma respectively and located in the GHS few kilometres to the South of the study area (Fig. 1) (CAROSI *et alii*, 2006).
The three analysed samples (Table 1) have similar geochemistry to that of the typical leucogranite in the GHS (VISONÀ & LOMBARDO, 2002; VISONÀ *et alii*, 2012) They are peraluminous leucogranite with an ASI (molecular ratio of $Al_2O_3/(CaO+Na_2O+K_2O)$) of 1.11-1.15 and a B value (Fe+Mg+Ti, DEBON & LE FORT, 1983))<40. Tourmaline granite 10-56 shows a flat REE pattern characterized by a marked Eu anomaly, and high concentrations of B, Be and of the most incompatible LILES (Cs and Rb) (Fig. 5). Moreover sample 10-56 shows higher contents of compatible elements such as Nb, U, Ta, W and Sn (Fig. 5) with respect to the two-mica granites (samples 10-41, this study and sample 10-53 from CAROSI *et alii*, 2006). Similarly to the two-mica leucogranites of the GHS (VISONÀ & LOMBARDO, 2002), the two-mica leucogranites presented here show a steeper REE pattern with a less pronounced Eu anomaly, and higher contents of less incompatible LILE (Sr and Ba), Pb and Th (Fig. 5). The only remarkable difference between the analysed granite and the two-mica granite of the GHS is the higher content of Ba (1246 ppm), Pb (127.7 ppm) and Sr (238 ppm) (Table 1).

Thermometry based on accessory monazite and zircon (WATSON & HARRISON, 1983; MONTEL, 1993) gives T_{REE} and T_{Zr} temperatures of 819-887°C °C and 731-797 °C, respectively. As the

granite contains inherited zircon and monazite (see below) these are maximum temperatures only.

Geochronology

Monazite and zircon were recovered after rock crushing and heavy liquid and magnetic separation. The grains were mounted in epoxy resin and polish down to expose their near equatorial section. Cathodoluminescence (CL) for zircon and backscattered electron (BSE) images for monazite were carried out on a scanning electron microscope (SEM) at the Australian National University (ANU) in Canberra. Operating conditions for the SEM were 15 kV/60 μA and 20 mm working distance. Imaging revealed that zircon contains only rare and thin overgrowths that have oscillatory zoning and likely formed during emplacement of the granite. Because of their small size (<30μm) and low abundance the zircon rims were not dated. Monazite is more abundant and crystals are generally euhedral and show a weak, oscillatory and polygonal zoning parallel to the crystal faces. A number of crystals are homogeneous in BSE images and others have small BSE-bright cores.

Monazite was analysed for U, Th and Pb isotopes using the sensitive high resolution ion microprobe (SHRIMP II) at the ANU. Instrumental conditions and data acquisition were generally as described by WILLIAMS (1998) and energy filtering (RUBATTO *et alii*, 2001) was applied to remove interferences and reduce matrix effects. The measured $^{206}Pb/^{238}U$ ratio was corrected using reference monazite USGS44069 (425 Ma, ALEINIKOFF *et alii*, 2007). The analyses were corrected for common Pb based on the measured $^{207}Pb/^{206}Pb$ according to the method of WILLIAMS (1998). See below for discussion of the possible effect of excess ^{206}Pb. U-Pb data were collected over one analytical session having calibration errors of 1.8% (2 sigma), which was propagated to single analyses. The common Pb composition was assumed to be that predicted by STACEY AND KRAMERS (1975) model. Data evaluation and age calculation were done using the software Squid 1 and Isoplot/Ex (LUDWIG 2003), respectively. Average ages are quoted at 95% confidence level (c.l.).

Homogeneous or oscillatory-zoned monazites have similar U, Th and Pb isotopic composition (Table 1). Nine analyses out of 11 form a cluster that defines and age of 13.9±06 Ma (MSWD 1.6) (Fig. 6). The few BSE-bright cores have much higher U content (15–18,000 ppm) and lower Th/U (5.6–13). Three analyses out of four define a good correlation line with an age of 15.8±0.3 (MSWD 0.42) (Fig. 6). With relatively young Th-rich phases, there is the possibility

that excess ^{206}Pb, derived from the decay chain of Th, affects the $^{206}Pb/^{238}U$ age. This has been documented in Himalayan granites (SCHÄRER, 1984), but is much less common in migmatites (RUBATTO *et alii* 2013). Excess ^{206}Pb can be detected by comparing $^{206}Pb/^{238}U$ ages with $^{207}Pb/^{235}U$ or $^{208}Pb/^{232}Th$ ages. In the investigated sample, $^{207}Pb/^{235}U$ ages are always within error of the $^{206}Pb/^{238}U$ ages, but they are imprecise and thus not a good enough test for excess ^{206}Pb. Measured $^{208}Pb/^{232}Th$ ages are systematically 10-15% younger than $^{206}Pb/^{238}U$ ages. This discrepancy could however be aggravated by the ion microprobe set up that is optimized for U-Pb ages and does not necessarily measure accurately the large Th signal. Therefore, in the absence of other independent constraints, the calculated $^{206}Pb/^{238}U$ ages are to be taken as maximum ages and the geological interpretation has to bear in mind that the actual age of monazites in the dike could be 1.4 to 2.1 Ma younger.

The oscillatory zoning in the main monazite domain suggests crystallization from a magma and thus their age of 13.9±0.6 Ma is interpreted as dating the maximum age of granite emplacement. The monazite cores that yield an older age are considered inherited to the magma and either crystallized from a previous batch of magma or were digested from the country or source rock.

Discussion and conclusion

The investigated leucogranites occupy a system of high-angle fractures (striking nearly E-W and dipping 80° to the north) that developed in the sillimanite-bearing gneiss of the upper GHS, just below the STDS in Western Bhutan. The high-angle fractures are hybrid-type, showing both nearly horizontal extension and a component of shear parallel to the walls. In Mohr space, hybrid fractures develop under very low confining pressure where Mohr circle approaches the tensile field (Fig. 7). The emplacement of leucogranites along these fractures testifies to the occurrence of melt migrating upward, filling the space opened by the extensional component of deformation at ~ 14 Ma and possibly as young as 12 Ma. The close relation between hybrid fractures (or "dilatant shear fractures") and melt emplacement has been recognized by DAVIDSON *et alii* (1994) and ANDRONICOS *et alii* (2003) in the migmatites of the Central Gneiss Belt (British Columbia, Canada). According to DAVIDSON *et alii* (1994) this could even indicate the simultaneous activity of deformation mechanisms provoking both

brittle and ductile behaviour within the same outcrop due to melt-enhanced embrittlement. The origin of the studied hybrid fractures can be related to the evolution of STD deformation from the ductile to the brittle realm. The hybrid fractures showing both nearly N-S extension and top-to-the North sense of shear developed at a small angle to the nearly vertical principal stress σ 1 in the footwall rocks of the STDS. This hybrid behaviour indicates an evolution toward lower confining pressure of the host-rocks previously deformed under medium- to high-grade metamorphic conditions. Up to ~ 14 Ma the upper GHS and the overlying Chekha formation were affected by ductile top-to-the North shearing under higher temperature conditions (KELLETT *et alii*, 2010) at which extensive fracture development is unlikely. On the other hand extension along the STD progressively brought the hot rocks in the footwall toward the surface at lower confining pressure. The occurrence of a km-scale system of hybrid fractures filled by leucogranites in high-grade rocks further testifies the exhumation of the hot footwall rocks.

We propose that exhumed "hot rocks" in the footwall of the STDS produced melt for several Ma since ~ 20 Ma , (sample 10-56 in CAROSI et *alii* 2006; Fig. 2). This melt migrated upward and was emplaced in the new opening sub-vertical fractures. As the melt cooled down, active shear deformation occurred in the solid-state condition with the development of mylonites showing a top-to-the North sense of shear, nearly contemporaneous with the fractures.

According to VISONÀ & LOMBARDO (2002), prograde metamorphism of micas-rich metapelitic source in the GHS produced both types of leucogranite found in the study area: tourmaline leucogranite at lower temperature and two mica leucogranite at higher temperature. The first anatectic melts correspond to tourmaline leucogranite sample 10-56 which formed at ~ 20 Ma (CAROSI *et alii* 2006; Fig. 2) by dehydration melting of muscovite occured at relatively lower T with respect to melting involving biotite (i.e. sample 10-53 at ~ 17 Ma in CAROSI *et alii* 2006). Melts at 20-17 Ma emplaced in top-to-the South normal-sense shear zones have been linked to the ductile extrusion of the core of the GHS (CAROSI *et alii* 2006; Fig. 2).

The leucogranite emplaced in the hybrid fracture of Limithang at ~ 14-12 Ma (sample 10-41) shows a similar composition to the two-mica leucogranite emplaced at ~17 Ma in the nearby GHS (CAROSI *et alii* 2006; Fig. 2). Moreover, the monazite relict cores in the sample 10-41 yield ages up to 15.8±0.3 Ma, close to the ~17 Ma age of the other two-mica leucogranite. We speculate that melting of muscovite-rich metapelites to produce two-mica leucogranite lasted from 17 to 14 Ma and possibly as late as 12 Ma in the upper GHS of Western Bhutan. This is in

line with protracted melting within the GHS documented in several sections of the Himalaya: the Leo Pargil dome of northwestern India (LEDERER *et alii,* 2013), the Annapurna and Nyalam regions of central Nepal (KOHN & CORRIE, 2011; WANG et *alii*, in press), east-central Nepal (LARSON et *alii*, 2011), the Mount Everest region (COTTLE et *alii*, 2009), eastern Nepal (IMAYAMA et *alii*, 2012) and Sikkim (RUBATTO et *alii,* 2013). Our findings are also in good agreement with the recent results of zircon U-Th-Pb analysis on deformed leucogranites and metapelites from the footwall of the STD in Western Bhutan where metamorphism and deformation related to STD displacement continued until ~ 14 Ma (COOPER *et alii*, in press).

The occurrence and the geometry of the hybrid fractures is however just above the inferred trace of the Laya Thrust (GRUJIC *et alii*, 2011) the trace of which is just south of the study area (Fig. 2). This could suggest an alternative hypothesis in which hybrid fractures are interpreted as Riedel antithetic fractures related to the top-to-the South out of sequence Laya thrust. The sense of shear is consistent with the orientation of Riedel antithetic fractures. Anyway Riedel fractures are shear fractures without the extensional component occurring in the recognized hybrid type and, in addition, the fractures should dip to the South, whereas they actually dip to the North. These considerations rule out a link between hybrid fractures and the Laya thrust.

KELLETT *et alii* (2009) dated the ductile Inner STDS at ~ 13-11 Ma so that the hypothesis of linking the hybrid fractures to stress field related the STDS activity is in good agreement with it. In this case the rotation due to the later antiform should be very small with a low amplitude.

The occurrence of large-scale antiforms and synforms affecting the GHS, TSS as well as the STDS and MCT (CAROSI *et alii*, 1999; UPRETI, 1999; KELLETT *et alii*, 2010) prevented the continuation of shearing along the STDS because movements along curved shear zones became very difficult. According to KELLETT *et alii* (2009) shearing along STDS stopped in the outer part of the belt and migrated in the inner part at 11 Ma. Therefore we conclude that the age of the sheared dykes in the inner part of the belt at ca. 14-12 Ma predates the age of orogen-parallel large-scale antiforms and synforms affecting the outer part of the Himalayan belt.

Acknowledgements

Financial support was provided by project MIUR-PRIN 2010-2011 (Resp. R. Carosi) and by Pisa (Resp. C. Montomoli), Torino (Resp. R. Carosi) and Padova (Resp. D. Visonà) Universities.

References

ANDRONICOS, C.L., CHARDON, D., GEHRELS, G., HOLLISTER, L.S., WOODSWORTH, G.J. (2003) – *Strain partitioning in an obliquely convergent orogen, plutonism, and synorgenic collapse: the Coast Mountains Batholith, British Columbia, Canada*. Tectonics **22**. doi:10.1029/2001TC001312.

ALEINIKOFF J.N., SCHENCK W.S., PLANK M.O., SROGI L., FANNING C.M., KAMO S.L. & HOWELL B. (2007) – *Deciphering igneous and metamorphic events in high-grade rocks of the Wilmington Complex, Delaware: Morphology, cathodoluminescence and backscattered electron zoning, and SHRIMP U-Pb geochronology of zircon and monazite.* Geological Society of America Bulletin, **118**, 39–64,

BEAUMONT C., JAMIESON R.A., NGUYEN M.H. & LEE, B. (2001) – *Himalayan tectonics explained by extrusion of a low-viscosity crustal channel coupled to focused surface denudation.* Nature, **414**, 738–742.

BURCHFIEL B.C., ZHILIANG C., HODGES K.V., YUPING L., ROYDEN L.H., CHANGRON D. & JIENE X. (1992) – *The South Tibetan Detachment System, Himalayan Orogen.* Geological Society of America Special Paper, **269**, 41 pp.

BURG J.P., BRUNEL M., GAPAIS D., CHEN G.M. & LIU G.H. (1984) – *Deformation of leucogranites of the crystalline Main Central Sheet in southern Tibet (China).* Journal of Structural Geology, **6**, 535–542.

CABY R., PÊCHER A. & LE FORT P. (1983) – *Le grand chevauchement central himalayen: Nouvelles données sur le métamorphisme inverse à la base de la Dalle du Tibet*. Revue de Géologie Dynamique et de Géographie Physique, **24**, 89–100.

CAROSI R., LOMBARDO B., MOLLI G., MUSUMECI G. & PERTUSATI P.C. (1998) – *The south Tibetan detachment system in the Rongbuk valley, Everest Region. Deformation features and geological implication*. Journal of Asian Earth Sciences, **16**, 299–311.

CAROSI R., MONTOMOLI C. & VISONÀ D. (2006) – *Normal sense shear zones in the core of higher Himalayan Crystallines (Bhutan Himalaya): evidence for extrusion?* Geological Society, London, Special Publications, **268**, 425-444.

CAROSI R., MONTOMOLI C., LANGONE A., TURINA A., CESARE B., IACCARINO S., FASCIOLI L., VISONÀ D., RONCHI A. & RAI S.M. (2015) – *Eocene partial melting recorded in peritectic garnets from*

kyanite-gneiss, Greater Himalayan Sequence, central Nepal. Geological Society, London, Special Publications, **412**, 111-129, doi:10.1144/SP412.1

CAROSI R., MONTOMOLI C., RUBATTO D. & VISONÀ D. (2013) – *Leucogranite intruding the South Tibetan Detachment in western Nepal: implications for exhumation models in the Himalayas*. Terra Nova, **25**, 278-489.

CAROSI R., LOMBARDO B., MUSUMECI G. & PERTUSATI P.C. (1999) – *Geology of the Higher Himalayan Crystallines in Khumbu Himal (Eastern Nepal).* Journal of Asian Earth Sciences, **17**, 785-803.

COOPER F.J., HODGES K.V., PARRISH R.R., ROBERTS N.M.W. & HORSTWOOD M.S.A. *in press.* – *Synchronous N-S and E-W extension at the Tibet-to-Himalaya transition in NW Bhutan.* Tectonics, DOI: 10.1002/2014TC003712

COTTLE J.M., JESSUP M.J., NEWELL D.L., SEARLE M.P., LAW R.D. & HORSTWOOD M.S.A. (2007) – *Structural insights into the early stages of exhumation along an orogen-scale detachment: The South Tibetan Detachment System, Dzakaa Chu section, Eastern Himalaya.* Journal of Structural Geology, **29**, 1781-1797.

COTTLE J.M., SEARLE, M.P., HORSTWOOD, M. & WATERS, D.J. (2009) - *Midcrustal metamorphism, melting, and deformation in the Mount Everest region of Southern Tibet revealed by U(-Th)-Pb geochronology*. The Journal of Geology, **117**, 643-664.

COTTLE J.M., SEARLE M.P., JESSUP M.J., CROWLEY J.L. & LAW R.D. (2015) – *Rongbuk re-visited: Geochronology of leucogranites in the footwall of the South Tibetan Detachment System, Everest Region, Southern Tibet*. Lithos, **227**, 94-106.

DANIEL C.G., HOLLISTER L.S., PARRISH R.R. & GRUJIC D. (2003) – *Exhumation of the Main Central Thrust from lower crustal depths, eastern Bhutan Himalaya.* Journal of Metamorphic Geology, **21**, 317–334.

DAVIDSON C., SCHMID S. M., & HOLLISTER L. S. (1994) - *Role of melt during deformation in the deep crust*. TerraNova, **6**, 133 – 142.

DAVIDSON C., GRUJIC D., HOLLISTER L.S. & SCHMIDT S.M. (1997) – *Metamorphic reactions related to decompression and synkinematic intrusion of leucogranite, High Himalayan Crystallines, Bhutan*. Journal of Metamorphic Geolology, **15**, 593-612.

DEBON F. & LE FORT P. (1983) – *A chemical–mineralogical classification of common plutonic rocks and associations.* Transactions of the Royal Society of Edinburgh: Earth Sciences, **73**, 135-149.

DEBON F., LE FORT P., SHEPPARD S.M.F. & SONET J. (1986) – *The Four Plutonic Belts of the Transhimalaya-Himalaya: a Chemical, Mineralogical, Isotopic, and Chronological Synthesis along a Tibet-Nepal Section*. Journal of Petrology, **27**, 219-250.

EDWARDS M.A. & HARRISON T.M. (1997) – *When did the roof collapse? Late Miocene north-south extension in the high Himalaya revealed by Th-Pb monazite dating of the Khula Kangri granite* Geology, **25**, 543-546.

GANSSER A. (1964) – *Geology of the Himalaya.* Wiley- Interscience, New York. 289 pp.

GANSSER A. (1983) – *Geology of the Bhutan Himalaya*. Birkhäuser Verlag, Basel-Boston-Stuttgart. 181 pp.

GOSCOMBE, B., D. GRAY, & M. HAND (2006) - *Crustal architecture of the Himalayan metamorphic front in eastern Nepal*. Gondwana Research doi:10.1016/j.gr.2006.05.003.

GRUJIC D., CASEY M., DAVIDSON C., HOLLISTER S.L., KÜNDIG R., PAVLIS T. & SCHMID S. (1996) – *Ductile extrusion of the Higher Himalayan Crystalline in Bhutan: evidence from quartz microfabrics*. Tectonophysics, **260**, 21–43.

GRUJIC D., HOLLISTER L. & PARRISH R.R. (2002) – *Himalayan metamorphic sequence as an orogenic channel: insight from Bhutan*. Earth and Planetary Science Letters, **198**, 177–191.

GRUJIC D., WARREN C.J. & WOODN J.L. (2011) – *Rapid synconvergent exhumation of Miocene-aged lower orogenic crust in the eastern Himalaya*. Lithospere, **3**, 346-366.

GUILLOT S., HODGES K., LE FORT P. & PÊCHER A. (1994) – *New constraints on the age of the Manaslu leucogranite: Evidence for episodic tectonic denudation in the central Himalayas*. Geology, **22**, 559-562

HARRIS N. & MASSEY J. (1994) – *Decompression and anatexis of Himalayan metapelites*. Tectonics, **13**, 1537–1546.

HODGES K.V., PARRISH R.R., HOUSH T.B., LUX D.R., BURCHFIEL B.C., ROYDEN L.H. & CHEN Z. (1992) – *Simultaneous Miocene extension and shortening in the Himalayan Orogen*. Science, **258**, 1466–1470.

IACCARINO S., MONTOMOLI C., CAROSI R., MASSONNE H.-J., LANGONE A., VISONÀ D. (2015) -*Pressure-temperature-time-deformation path of kyanite-bearing migmatitic paragneiss in the Kali Gandaki valley (Central Nepal): Investigation of Late Eocene-Early Oligocene melting processes.* Lithos, 231, 103-121.

IMAYAMA T., TAKESHITA T., YI K., CHO D.-L., KITAJIMA K., TSUTSUMI Y., KAYAMA M., NISHIDO H., OKUMURA T., YAGI K., ITAYA T. & SANO Y. (2012) – *Two-stage partial melting and contrasting cooling history within the Higher Himalayan Crystalline Sequence in the far-eastern Nepal Himalaya.* Lithos, **134-135**, 1-22.

JESSUP M.J., COTTLE J.M. SEARLE M.P. LAW R.D., NEWELL D.L., TRACY R.J. & WATERS D.J. (2008) – *P–T–t–D paths of Everest Series schist, Nepal.* Journal of Metamorphic Geology, **26**, 717-739.

KELLETT D., GRUJIC D. & ERDMANN S. (2009) – *Miocene structural reorganization of the South Tibetan detachment, eastern Himalaya: Implications for continental collision*. Lithosphere, **1**, 259-281.

KELLETT D., GRUJIC D., WARREN C., COTTLE J., JAMIESON R. & TENZIN T. (2010) – *Metamorphic history of a syn-convergent orogen-parallel detachment: The South Tibetan detachment system, Bhutan Himalaya.* Journal of Metamorphic Geology, **28**, 785-808.

KELLETT D. & GRUJIC D. (2012) - *New insight into the South Tibetan detachment system: Not a single progressive deformation*. Tectonics, doi:10.1029/2011TC002957.

KELLETT D.A., GRUJIC D., COUTAND I., COTTLE J. & MUKUL M. (2013) - *The South Tibetan detachment system facilitates ultra rapid cooling of granulite-facies rocks in Sikkim Himalaya*. Tectonics, 32, 252–270, DOI:10.1002/TECT.20014, 2013.

KING J., HARRIS N., ARGLES T., PARRISH R. & ZHANG H. (2011) – *Contribution of crustal anatexis to the tectonic evolution of Indian crust beneath southern Tibet.* Geological Society of America Bulletin, **123**, 218–239.

KOHN M.J. (2008) – *P-T-t data from Nepal support critical taper and repudiate large channel flow of the Greater Himalayan Sequence.* Geological Society of America Bulletin, **120**, 259–273.

KOHN M.J. & CORRIE S.L. (2011) - *Preserved Zr-temperatures and U–Pb ages in high-grade metamorphic titanite: Evidence for a static hot channel in the Himalayan orogen*. Earth and Planetary Science Letters, **311**, 136-143.

LARSON K.P. & GODIN L. (2009) – *Kinematics of the Greater Himalayan sequence, Dhaulagiri Himal: implications for the structural framework of central Nepal.* Journal of the Geological Society, **166**, 25-43.

LARSON K., COTTLE J.M. & GODIN L. (2011) – *Petrochronologic record of metamorphism and melting in the upper Greater Himalayan sequence, Manaslu-Himal Chuli Himalaya, west-central Nepal*. Lithosphere, **3**, 379-392.

LEDERER G.W., COTTLE J.M., JESSUP M.J., LANGILLE J.M. & AHMAD T. (2013) - *Timescales of partial melting in the Himalayan middle crust: insight from the Leo Pargil dome, northwest India.* Contributions to Mineralogy and Petrology, **166**, 1415-1441.

LEECH M.L. (2008) – *Does the Karakoram fault interrupt mid-crustal channel flow in the western Himalaya?* Earth and Planetary Science Letters, **276**, 314-322.

LONG S., MCQUARRIE N., TOBGAY T., GRUJIC D. & HOLLISTER L. (2011) – *Geologic Map of Bhutan.* Journal of Maps, **7**, DOI: 10.4113/jom.2011.1159

LUDWIG K.R. (2003) – *Isoplot/Ex version 3.0. A geochronological toolkit for Microsoft Excel.*

Berkeley Geochronology Center, Special Publications, 4.

MONTOMOLI C., IACCARINO S., CAROSI R., LANGONE A. & VISONÀ D. (2013) – *Tectonometamorphic discontinuities within the Greater Himalayan Sequence in Western Nepal (Central Himalaya): insights on the exhumation of crystalline rocks*. Tectonophysics, **608**, 1349–1370.

MONTOMOLI C., CAROSI R. & IACCARINO S. (2015) – *Tectonometamorphic discontinuities in the Greater Himalayan Sequence: a local or a regional feature?* Geological Society, London, Special Publications, **412**, 25-41, doi:10.1144/SP412.3

PATIÑO-DOUCE A., & HARRIS N. (1998) – *Experimental constraints on Himalayan anatexis*. Journal of Petrology, **39**, 689–710.

RAMSEY J.M. & CHESTER F.M. (2004) – *Hybrid fracture and the transition from extension fracture to shear fracture*. Nature, **428**, 63-66.

RUBATTO D., CHAKRABORTY S. & DASGUPTA S. (2013) - *Timescales of crustal melting in the Higher Himalayan Crystallines (Sikkim, Eastern Himalaya) inferred from trace element-constrained monazite and zircon chronology.* Contribution to Mineralogy and Petrology, **165**, 349-372.

RUBATTO D., WILLIAMS I.S. & BUICK I. (2001) – *Zircon and monazite response to prograde metamorphism in the Reynolds Range, central Australia.* Contributions to Mineralogy and Petrology, **140**, 458-468.

SCHÄRER U. (1984) - *The effect of initial ^{230}Th disequilibrium on young U-Pb ages: the Makalu case, Himalaya*. Earth Planetary Science Letters, **67**, 191-204

SEARLE M.P. (1999) – *Extensional and compressional faults in the Everest–Lhotse massif, Khumbu Himalaya, Nepal*. Journal of the Geological Society, **156**, 227-240.

SEARLE M.P. (2013) – *Crustal melting, ductile flow, and deformation in mountain belts: Cause and effect relationships*. Lithospere, doi:10.1130/RF.L006.1.

SEARLE M.P. & GODIN L. (2003) – *The south Tibetan detachment and the Manaslu Leucogranite: A structural reinterpretation and restoration of the Annapurna-Manaslu Himalaya, Nepal.* The Journal of geology, **111**, 505-523.

SEARLE M.P., COTTLE J.M., STREULE M.J. & WATERS D.J. (2010) – *Crustal melt granites and migmatites along the Himalaya: melt source, segregation, transport and granite emplacement mechanisms.* Geological Society of America Special Papers, **472**, 219-233.

SINGHAL B.B.S. & GUPTA R. P. (2010) – *Applied hydrogeology of fractured rocks, second edition*, 408 pp. ISBN 978-90-481-8798-0.

STACEY J.S. & KRAMERS J.D. (1975) – *Approximation of Terrestrial Lead Isotope Evolution by a 2-Stage Model.* Earth and Planetary Science Letters, **26**, 207-221.

STREULE M.J., SEARLE M.P., WATERS D.J. & HORSTWOOD M.S.A. (2010) – *Metamorphism, melting, and channel flow in the Greater Himalayan Sequence and Makalu leucogranite: Constraints from thermobarometry, metamorphic modeling, and U-Pb geochronology*. Tectonics, **29**, DOI: 10.1029/2009TC002533

UPRETI B.N. (1999) – *An overview of the stratigraphy and tectonics of the Nepal Himalaya*. Journal of Asian Earth Sciences, **17**, 577-606.

VANNAY J.C. & GRASEMANN B. (2001) – *Himalayan invertedmetamorphismand synconvergence extension as a consequence of a general shear extrusion.* Geological Magazine, **138**, 253–276.

VISONÀ D. & LOMBARDO B. (2002) – *Two-mica and tourmaline leucogranites from Everest–Makalu region (Nepal–Tibet). Himalayan leucogranites genesis by isobathic heating?* Lithos, **62**, 125–150.

VISONÀ D., CAROSI R., MONTOMOLI C., PERUZZO L. & TIEPOLO M. (2012) – *Miocene andalusite leucogranite in central-east Himalaya (Everest–Masang Kang area): low-pressure melting during heating.* Lithos ,**144**, 194–208.

WANG J.-M., RUBATTO D. & ZHANG J.-J. (2015) - *Timing of partial melting and cooling across the Greater Himalayan Crystalline Complex (Nyalam, central Himalaya): in-sequence thrusting and its implications.* Journal of Petrology, in press

WEBB A.A.G., YIN A., HARRISON T.M., CÉLÉRIER J. & BURGESS P.W. (2007) – *The leading edge of the Greater Himalayan Crystalline complex revealed in the NW Indian Himalaya: implications for the evolution of the Himalayan orogen.* Geology, **35**, 955–958.

WILLIAMS I.S. (1998) – *U–Th–Pb geochronology by ion microprobe.* Reviews in Economic Geology, **7**, 1–35.

Figures captions

Fig. 1 – A: Geological sketch map of the Himalaya, with location of study area (after GANSSER, 1964 and LAW et *alii*, 2004). A. SSZ= Shyok suture zone; ZSZ: Zanskar shear zone; MKT: Main Karakoram Thrust; MMT: Main Mantle Thrust; TB: Tibetan Block; ITSZ: Indus Tsangpo Suture Zone; GCT: Great Counter Thrust; TSS: Tibetan Sedimentary Sequence; GHS: Greater Himalayan Sequence; STDS: South Tibetan Detachment System; MCT: Main Central Thrust; MBT: Main Boundary Thrust; MFT: Main Frontal Thrust; K: Kashmir basin; P: Peshawar basin; S: Sutlej basin. B: NS cross section of the Himalayan belt.

Fig. 2 – Geological sketch map of the Thimpu-Laya area (modified from GANSSER, 1983; GRUJIC *et alii*, 2002; 2011; CAROSI *et alii*, 2006; LONG *et alii*, 2011). 1: Quaternary; 2: Tethyan Sedimentary Sequence; 3: Chekha Formation; 5: Greater Himalyan Sequence; 5: High Himalayan Leucogranite; 6: mafic pods; 7: Calcsilicates GHS; 8: Paro Formation; 9: Marble (of the Paro Formation); 10: main foliation; 11: main sillimanite lineation; 12: Thrust faults (LT: Laya Thrust , MCT: Main Central Thrust); 13: Inner South Tibetan Detachment (I-STDS); 14: Outer South Tibetan Detachment (O-STDS); 15: Normal faults (YF: Yadong fault); 16: Synform; 17: Antiform; 18: Sample location (this study); 19: Sample after Carosi *et alii*, 2006.

Fig. 3A, B - High-angle hybrid fractures (striking nearly E-W and dipping 80° to the north) filled by mylonitic leucogranites occur in the highest portion of the GHS, just below the STD (view to east).

Fig. 4 – A: Shear sense indicators (mica fish) point to a top-down-to-the-North sense of shear (FOV is 0.8 mm) in mylonitic leucogranites (B) (in the present position). FOV is 1 cm.

Fig. 5 – Rare Earth Element plot of the study sample 10-41 (Limithang) compared to the other two leucogranite samples from CAROSI *et alii* (2006).

Fig. 6 - SHRIMP U-Pb analyses of monazite plotted on a Tera-Wasserburg diagram (left) and representative BSE images of dated crystals (right)

Fig. 7. Hybrid fractures in the Mohr space developed in low normal stress condition (left side of the diagram) (redrawn from SINGHAL & GUPTA, 2010).

Table 1. Geochemical composition of leucogranite dikes

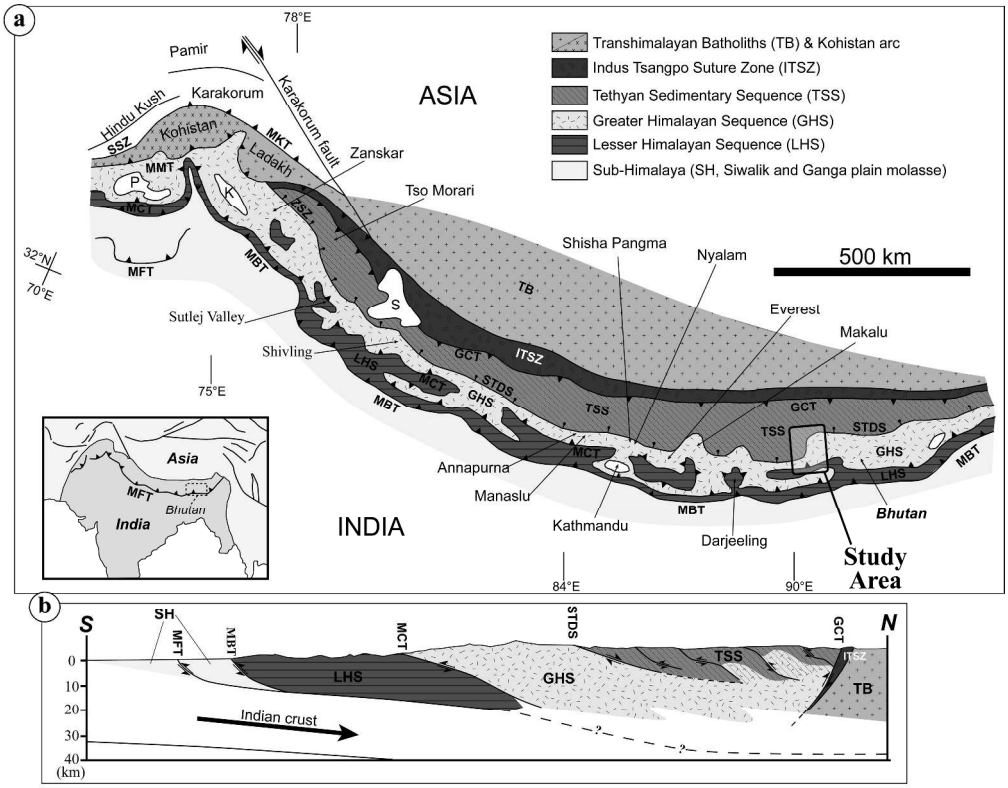

Fig. 1 – A: Geological sketch map of the Himalaya, with location of study area (after GANSSER, 1964 and LAW et alii, 2004). A. SSZ= Shyok suture zone; ZSZ: Zanskar shear zone; MKT: Main Karakoram Thrust; MMT: Main Mantle Thrust; TB: Tibetan Block; ITSZ: Indus Tsangpo Suture Zone; GCT: Great Counter Thrust; TSS: Tibetan Sedimentary Sequence; GHS: Greater Himalayan Sequence; STDS: South Tibetan Detachment System; MCT: Main Central Thrust; MBT: Main Boundary Thrust; MFT: Main Frontal Thrust; K: Kashmir basin; P: Peshawar basin; S: Sutlej basin. B: NS cross section of the Himalayan belt.
334x268mm (300 x 300 DPI)

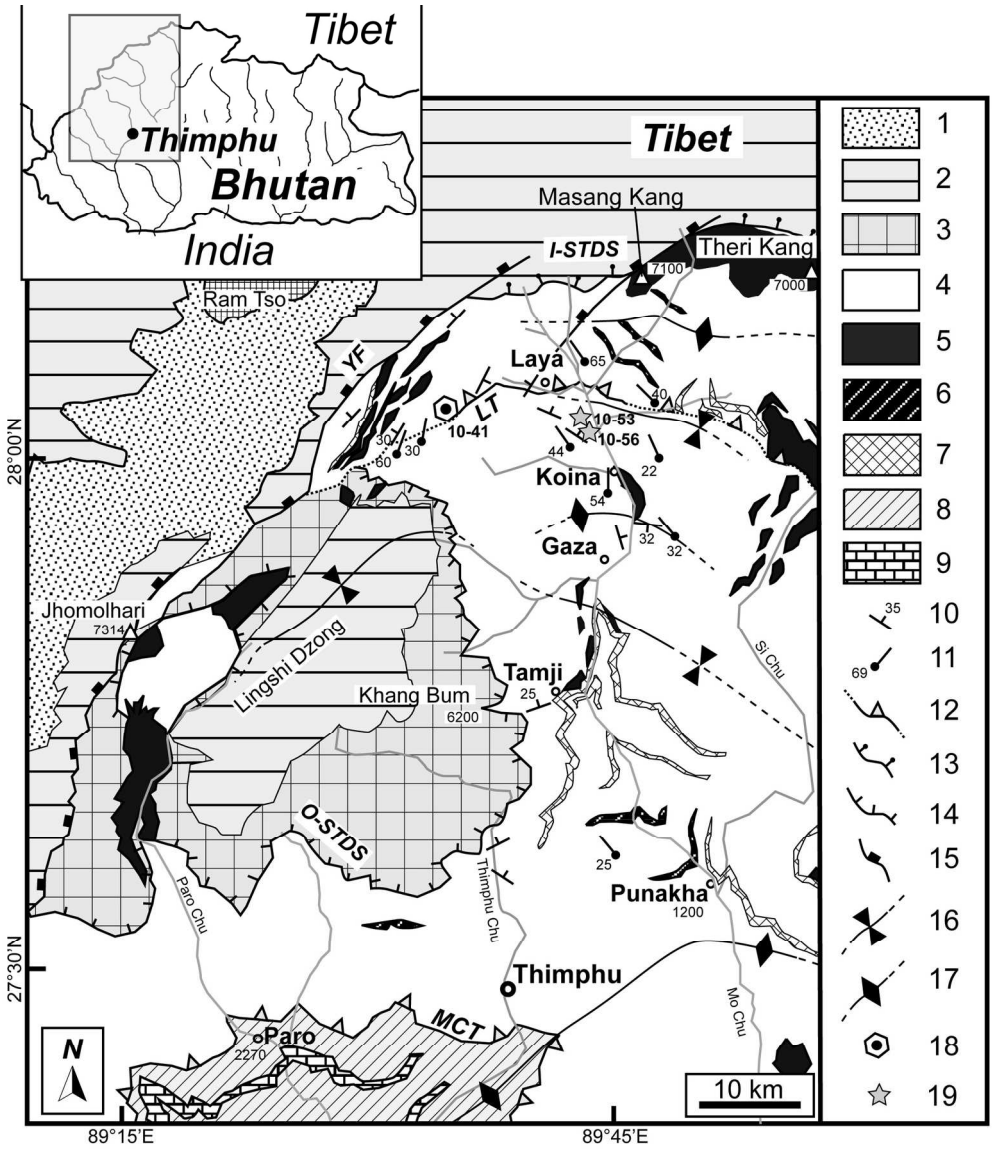

Fig. 2 – Geological sketch map of the Thimpu-Laya area (modified from GANSSER, 1983; GRUJIC et alii, 2002; 2011; CAROSI et alii, 2006; LONG et alii, 2011). 1: Quaternary; 2: Tethyan Sedimentary Sequence; 3: Chekha Formation; 5: Greater Himalyan Sequence; 5: High Himalayan Leucogranite; 6: mafic pods; 7: Calcsilicates GHS; 8: Paro Formation; 9: Marble (of the Paro Formation); 10: main foliation; 11: main sillimanite lineation; 12: Thrust faults (LT: Laya Thrust , MCT: Main Central Thrust); 13: Inner South Tibetan Detachment (I-STDS); 14: Outer South Tibetan Detachment (O-STDS); 15: Normal faults (YF: Yadong fault); 16: Synform; 17: Antiform; 18: Sample location (this study); 19: Sample after Carosi et alii, 2006.
170x194mm (300 x 300 DPI)

Fig. 3A, B - High-angle hybrid fractures (striking nearly E-W and dipping 80° to the north) filled by mylonitic leucogranites occur in the highest portion of the GHS, just below the STD (view to east).
138x185mm (600 x 600 DPI)

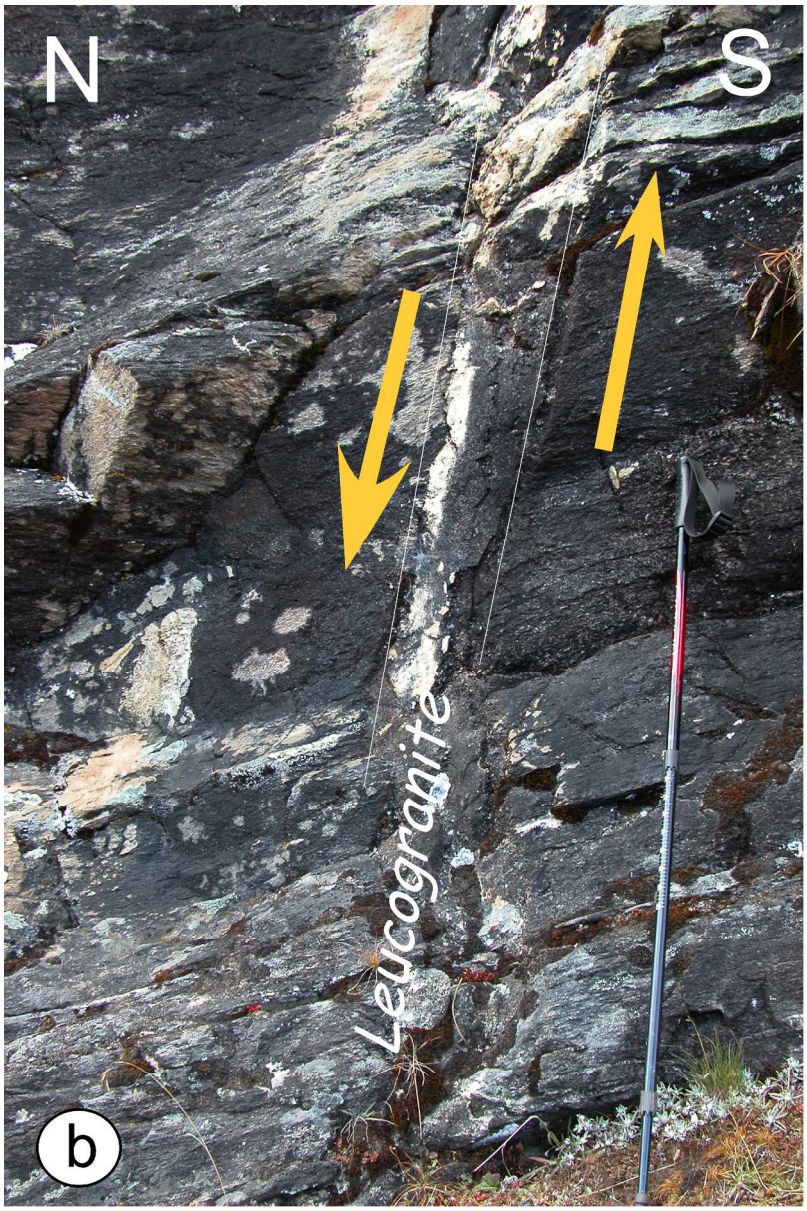

Fig. 3A, B - High-angle hybrid fractures (striking nearly E-W and dipping 80° to the north) filled by mylonitic leucogranites occur in the highest portion of the GHS, just below the STD (view to east).
118x177mm (600 x 600 DPI)

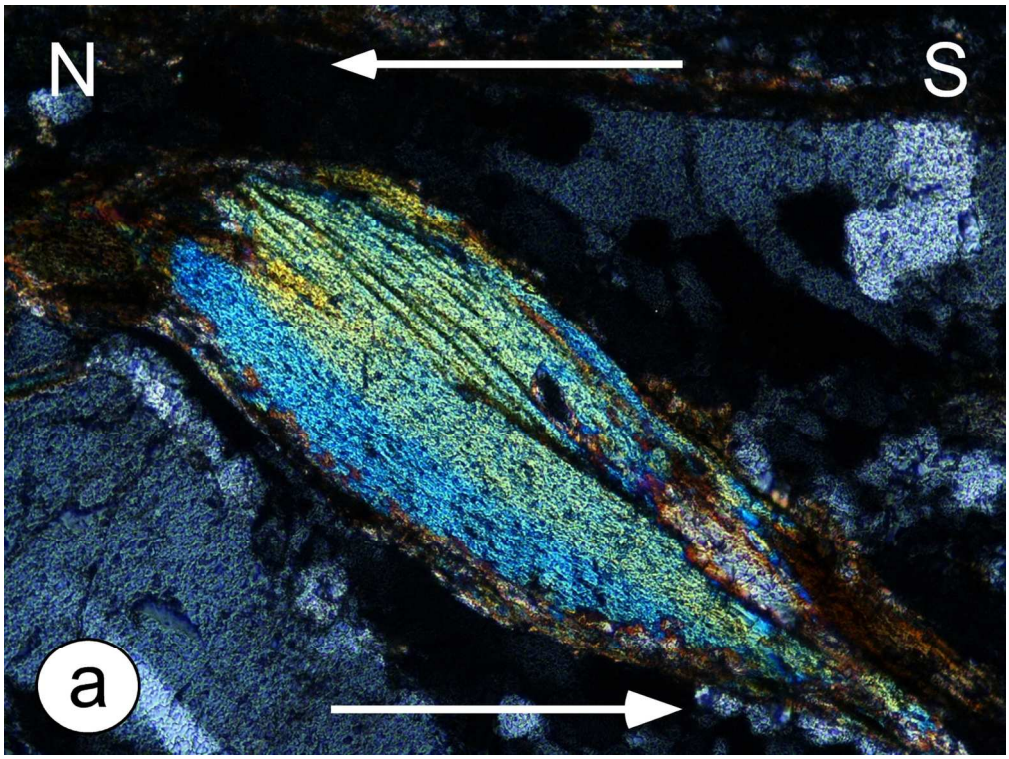

Fig. 4 – A: Shear sense indicators (mica fish) point to a top-down-to-the-North sense of shear (FOV is 0.8 mm) in mylonitic leucogranites (B) (in the present position). FOV is 1 cm.
68x51mm (600 x 600 DPI)

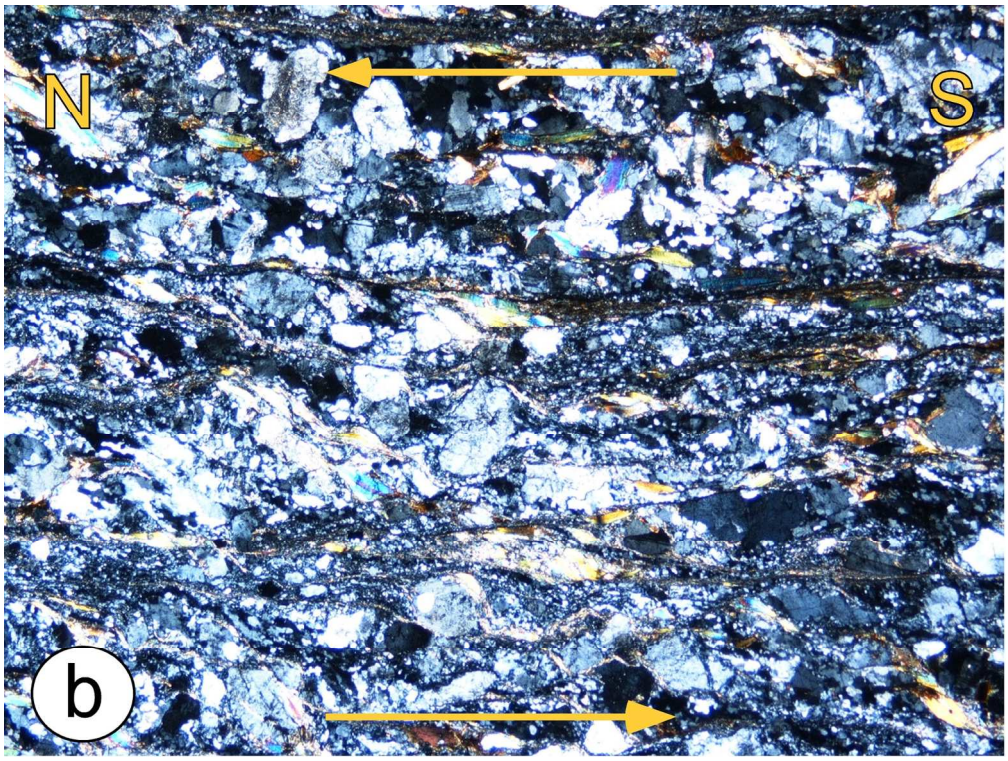

Fig. 4 – A: Shear sense indicators (mica fish) point to a top-down-to-the-North sense of shear (FOV is 0.8 mm) in mylonitic leucogranites (B) (in the present position). FOV is 1 cm.
77x57mm (600 x 600 DPI)

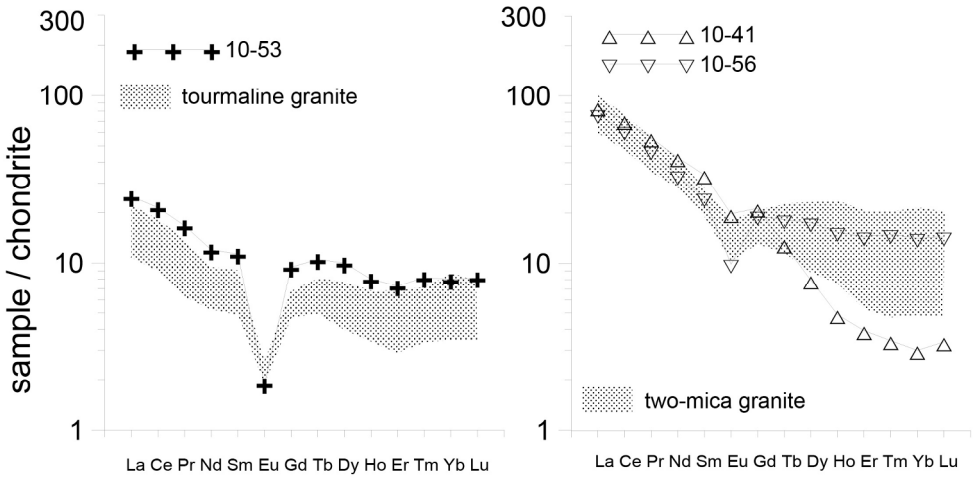

Fig. 5 – Rare Earth Element plot of the study sample 10-41 (Limithang) compared to the other two leucogranite samples from CAROSI et alii (2006).
193x93mm (300 x 300 DPI)

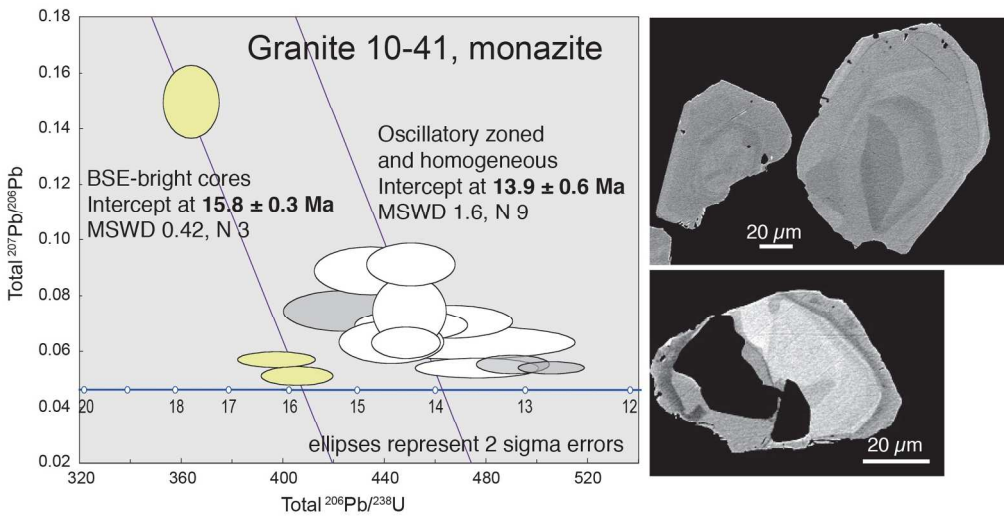

Fig. 6 - SHRIMP U-Pb analyses of monazite plotted on a Tera-Wasserburg diagram (left) and representative BSE images of dated crystals (right)
178x93mm (300 x 300 DPI)

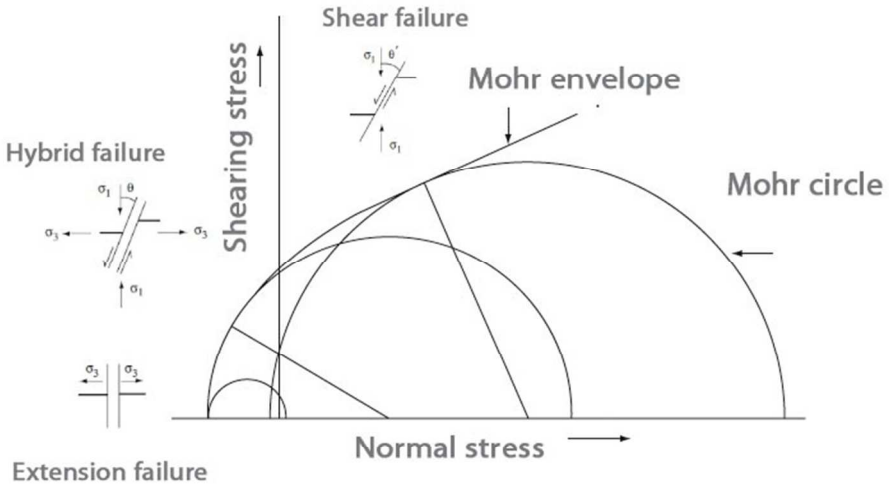

Fig. 7. Hybrid fractures in the Mohr space developed in low normal stress condition (left side of the diagram) (redrawn from SINGHAL & GUPTA, 2010).
66x36mm (300 x 300 DPI)

	10-41	10-53	10-56
SiO_2	73.44	73.63	75.48
Al_2O_3	15.18	15.11	14.34
Fe_2O_3	0.98	1.25	0.88
MnO	0.01	0.02	0.03
MgO	0.23	0.26	0.12
CaO	0.71	1.37	0.57
Na_2O	3.67	3.67	3.57
K2O	5.44	4.65	4.83
TiO_2	0.15	0.12	0.05
P_2O_5	0.06	0.13	0.08
PF	0.97	0.77	0.69
Total	100.84	100.97	100.62
Ba	1246	322.3	58.08
Be	4.062	3.95	11.1
Bi	2.044	0.286	8.976
Ce	57.68	49.95	17.36
Co	0.817	1.73	0.593
Cr	<5	6.395	< 5
Cs	18.82	7.144	39.14
Cu	<3	<3	<3
Dy	2.532	5.584	3.205
Er	0.826	3.03	1.529
Eu	1.385	0.692	0.132
Ga	18.67	18.06	24.84
Gd	5.543	4.984	2.46
Ge	1.478	1.818	3.158
Hf	1.429	3.15	1.919
Ho	0.343	1.073	0.561
La	26.58	23.97	7.751
Lu	0.101	0.432	0.245
Nb	7.677	10.67	24.75
Nd	25.76	20.08	7.198
Ni	< 4	< 4	< 4
Pb	127.70	71.60	52.16
Pr	6.741	5.662	2.005
Rb	190.2	229.1	469.7
Sb	0.966	< 0.2	0.226
Sm	6.781	4.924	2.266
Sn	4.753	3.658	18.23
Sr	238.9	132.6	22.58
Ta	1.668	2.214	13.77
Tb	0.652	0.91	0.526
Th	14.78	15.7	7.681
Tm	0.103	0.447	0.246
U	6.506	6.237	16.75
V	< 1.5	6.464	1.945
W	3.77	1.027	12.67
Y	10.42	34.33	19.35
Yb	0.631	2.968	1.674
Zn	32.21	32.22	28.75
Zr	45.91	99.98	47.51
ASI	1.15	1.11	1.18
B	18.72	22.08	13.39
T_monaz	845.00	819.00	750.00
Tzrn	731.00	794.00	701.00

$ASI=Al_2O_3/(CaO+Na_2O+K_2O)$

B=(Fe+Mg+Ti); Debon & Le Fort, 1983